



High-resolution simulation of link-level vehicle emissions and concentrations for air pollutants in a traffic-populated eastern Asian city

Shaojun Zhang^{1,2}, Ye Wu^{1,3}, Ruikun Huang¹, Jiandong Wang¹, Han Yan¹, Yali Zheng^{1,4}, and Jiming Hao^{1,3}

¹School of Environment and State Key Joint Laboratory of Environment Simulation and Pollution Control, Tsinghua University, Beijing 100084, P. R. China

²Department of Mechanical Engineering, University of Michigan, Ann Arbor, MI 48109, USA

³State Environmental Protection Key Laboratory of Sources and Control of Air Pollution Complex, Beijing 100084, P. R. China

⁴Society of Automotive Engineers of China, 102 Lianhuachi East Road, Beijing 100055, P.R. China

Correspondence to: Ye Wu (yw@tsinghua.edu.cn)

Received: 22 January 2016 – Published in Atmos. Chem. Phys. Discuss.: 4 February 2016

Revised: 27 June 2016 – Accepted: 15 July 2016 – Published: 9 August 2016

Abstract. Vehicle emissions containing air pollutants created substantial environmental impacts on air quality for many traffic-populated cities in eastern Asia. A high-resolution emission inventory is a useful tool compared with traditional tools (e.g. registration data-based approach) to accurately evaluate real-world traffic dynamics and their environmental burden. In this study, Macau, one of the most populated cities in the world, is selected to demonstrate a high-resolution simulation of vehicular emissions and their contribution to air pollutant concentrations by coupling multimodels. First, traffic volumes by vehicle category on 47 typical roads were investigated during weekdays in 2010 and further applied in a networking demand simulation with the TransCAD model to establish hourly profiles of link-level vehicle counts. Local vehicle driving speed and vehicle age distribution data were also collected in Macau. Second, based on a localized vehicle emission model (e.g. the emission factor model for the Beijing vehicle fleet – Macau, EMBEV–Macau), this study established a link-based vehicle emission inventory in Macau with high resolution meshed in a temporal and spatial framework. Furthermore, we employed the AERMOD (AMS/EPA Regulatory Model) model to map concentrations of CO and primary PM_{2.5} contributed by local vehicle emissions during weekdays in November 2010. This study has discerned the strong impact of traffic flow dynamics on the temporal and spatial patterns of vehicle emis-

sions, such as a geographic discrepancy of spatial allocation up to 26 % between THC and PM_{2.5} emissions owing to spatially heterogeneous vehicle-use intensity between motorcycles and diesel fleets. We also identified that the estimated CO₂ emissions from gasoline vehicles agreed well with the statistical fuel consumption in Macau. Therefore, this paper provides a case study and a solid framework for developing high-resolution environment assessment tools for other vehicle-populated cities in eastern Asia.

1 Introduction

The soaring vehicle stock driven by socio-economic development has created a series of substantial challenges regarding air pollution, energy insecurity, and public health within many countries (Uherek et al., 2010; Saikawa et al., 2011; Shindell et al., 2011; Walsh, 2014). At the national level, we take nitrogen oxides (NO_x) emissions as an example as it is an essential precursor to the formation of ozone and nitrate aerosol in the atmosphere. On-road vehicles are currently responsible for 29 % of national anthropogenic NO_x emissions in China (MEP, 2014), 37 % in US (US EPA, 2014) and 40 % in the European Union (EEA, 2014; Vestreng et al., 2009). At the city level, the vehicular contribution to ambient nitrogen dioxide (NO₂) concentration is very significant

in traffic-related areas (Carslaw et al., 2011). For example, in European countries where diesel vehicles make up a considerable part of private passenger cars, near-road NO_2 concentration exceeds the ambient air quality standard. This issue is seen as one of the most significant air pollution problems in Europe, although great efforts have been made to cope with the NO_2 exceedance, including the implementation of stringent emission standards for diesel vehicles (e.g. the latest Euro 6 requirements; Franco et al., 2014; Carslaw et al., 2011; Velders et al., 2011; Carslaw and Rhys-Tyler, 2013; Chen and Borcken-Kleefeld, 2014). Higher health risk as a result of exposure to vehicular emissions (e.g. particle, NO_x) is understandable in traffic-populated cities, and is probably associated with the large resident population, greater traffic congestion, and unfavourable dispersion due to dense buildings (Du et al., 2012; Ji et al., 2012). In 2012, the International Agency for Research on Cancer Group 1 assessed the carcinogenicity of diesel emissions as “carcinogenic to humans” with sufficient evidence for it to be characterized as a cause of lung cancer (Benbrahim-Tellaa et al., 2012).

The high-resolution vehicle emission inventory can be a valuable tool to accurately evaluate impacts on air quality and public health, as it can well reflect the close connections between environmental impacts and traffic flows. McDonald et al. (2014) analysed the impacts of enhanced spatial resolution from 10 km to 500 m on vehicular CO_2 emission inventory for Los Angeles, which clearly demonstrated substantial improvements in the accuracy for areas containing traffic-dense microenvironments (e.g. heavily trafficked highways). Consequently, link-based emission inventory is a preferred tool owing to its substantial advantage in spatial resolution for local traffic and environmental management. Over the past decade, high-resolution emission inventory initiatives have been carried out in China’s vehicle-populated cities. Taking Beijing, the capital city of China for example, Huo et al. (2009) established a link-based emission inventory for light-duty gasoline vehicles (LDGVs) in the urban area based on estimated emission factors with the IVE (International Vehicle Emissions) model. However, significant emissions of NO_x and fine particulate matter ($\text{PM}_{2.5}$) may be attributed to heavy-duty diesel vehicles (HDDVs) instead of LDGVs, including the gross emitters registered in other provinces (Wang et al., 2011, 2012), with contributions currently not evidenced in the registration-based inventories for China’s vehicle-populated cities (Wu et al., 2011; Zhang et al., 2014a; Zheng et al., 2015). Wang et al. (2009) and Zhou et al. (2010) estimated vehicular emissions for the urban area of Beijing by using grid-based data of average speed and aggregated vehicle kilometres travelled. However, their resolutions are not sufficient to present hourly fluctuations of network traffic volume and quantify vehicular emissions at the link level.

As traffic management actions become more important for vehicle emission control (Wu et al., 2016), such as the licence control policies effective in seven vehicle-populated

cities of China (e.g. Shanghai, Beijing, Guangzhou, Tianjin, etc.) and the Electronic Road Pricing (ERP) programme adopted in Singapore (Goh, 2002). We therefore envision greater demand for high-resolution vehicle emission inventories by local environmental protection administrations in the near future. A few technical barriers for improving the high-resolution vehicular emission inventory based on the development experience of the London Atmospheric Emission Inventory (LAEI; TfL, 2014) are expected to be shortly overcome. First, high-resolution traffic data including traffic counts, vehicle speed, and fleet composition should be investigated or estimated at the link level with hourly fluctuations. Second, real-world emission factors should be developed based on a sufficient measurement database to effectively address potential uncertainties (e.g. gaps between regulatory cycle and off-cycle conditions; Carslaw et al., 2011; Wu et al., 2012; Zhang et al., 2014a). Third, technology allocations of the total fleet (e.g. traffic counts by fuel type and vehicle age) should be derived based on real-world traffic data instead of registration data, considering vehicular emissions are fairly sensitive to vehicle technology allocations (Vallamsundar and Lin, 2012). Finally, the application of high-resolution emission inventory can be significantly enhanced by extending the evaluation framework from vehicular emissions to pollutant concentration, which are of overriding concerns to residents, pedestrians, and policy makers (Vallamsundar and Lin, 2012; Misra et al., 2013).

In this study, we selected Macau as a case city to demonstrate high-resolution simulation for vehicle emissions and primary concentrations of air pollutants in this traffic-populated city. Macau is well-renowned for its tourism and gambling industries, which attract numerous visitors and create a large transportation demand. Owing to the absence of a massive rail-based public transit system, which is now under construction in Macau, local transportation completely depends on on-road vehicles. The vehicle-population density (including motorcycles, MCs) in Macau is approaching 7800 veh km^{-2} in 2014, significantly more dense than other eastern Asian cities (e.g. 430 veh km^{-2} of Shanghai, 340 veh km^{-2} of Beijing and 700 veh km^{-2} of Hong Kong; DESC, 2014; HKS, 2014; NBSC, 2014). Furthermore, Macau’s total vehicle population has surpassed 240 000 in 2014, more than double the level in 2000 (DESC, 2014). Significant gridlock has been caused due to rapid motorization in the Macau Peninsula during rush hours, when the average speed of arterial roads is frequently lower than 15 km h^{-1} (TMB, 2010). On the other hand, local air quality data indicate several non-attainment sites for annual ambient $\text{PM}_{2.5}$ and NO_2 concentrations in the traffic-dense and residential areas of Macau (DESC, 2014). On-road vehicles have been identified as the major local contributor to air pollution, because industrial emissions in Macau are quite minor compared with the on-road transportation sector. Thus, there is an urgent need to attach importance to controlling vehicular

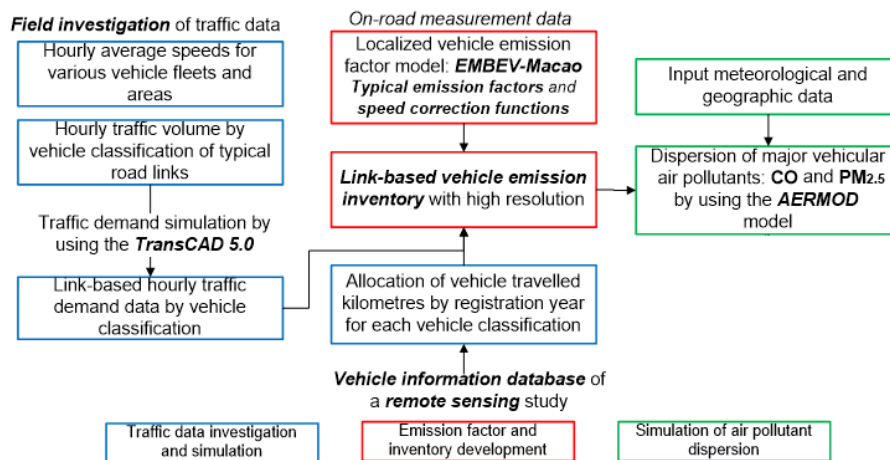


Figure 1. Framework of high-resolution simulation for vehicle emissions and concentrations of vehicular pollutants.

emissions with the support of high-resolution emission inventory technology in this traffic-populated city.

2 Methodology and data

2.1 General study framework and components

This study generally consists of three components: (1) characterizing hourly traffic profiles at the link level, (2) establishing a high-resolution vehicle emission inventory, and (3) simulating the concentrations of typical primary air pollutants (e.g. CO, PM_{2.5}) contributed by local vehicle emissions in Macau (see Fig. 1). The core task of this study is to calculate emissions of air pollutants and carbon dioxide (CO₂) from local vehicles meshed in the high-resolution matrix of the “hour-link-vehicle technology group”, which is illustrated by Eq. (1).

$$E_{h,l,p,v} = \sum_{f,y} 10^{-3} \cdot \text{EF}_{f,p,v,y} \cdot L_l \cdot \text{TV}_{h,l,v} \cdot \text{VF}_{f,v,y}, \quad (1)$$

where the emissions of pollutant category p are from vehicle classification v during hour h for link l , kg h^{-1} ; $\text{EF}_{f,p,v,y}$ is speed-dependent average emission factor of pollutant category p for vehicle technology group defined by classification v , fuel type f , and vehicle age y , $\text{g veh}^{-1} \text{km}^{-1}$; L_l is the total length of link l , km; $\text{TV}_{h,l,v}$ is total traffic volume of vehicle classification v during hour h , veh h^{-1} ; and $\text{VF}_{f,v,y}$ is the volume fraction of vehicle technology group (e.g. model year group) defined by fuel type f and vehicle age y . We define eight vehicle classifications in this study that were recognized from road traffic video records as follows: light-duty passenger vehicle (LDPV), MC, taxi, public bus (PB), medium-duty passenger vehicle (MDPV), heavy-duty passenger vehicle (HDPV), light-duty truck (LDT), and heavy-duty truck (HDT).

Therefore, we further characterized total hourly emissions from the total vehicle fleet based on the bottom-up method, namely from each link to the entire road net, as Eq. (2) illustrates.

$$E_{h,p} = \sum_{l,v} E_{h,l,p,v}, \quad (2)$$

where $E_{h,p}$ is the total vehicle emission of pollutant category p during hour h from the total vehicle fleet in Macau, kg h^{-1} . In the following two subsections, we present detailed methods for developing high-resolution traffic data and vehicle emission factors. Due to the time limitation on the traffic field investigation, we only focus the case study for weekdays in 2010; weekends when traffic flows might be different were not investigated.

2.2 Summary of geography and road network in Macau

Macau is one of the two special administrative regions (SAR) in China and lies on the western side of the Pearl River delta, with a total land area of only 30 km², which makes it the most densely populated city in the world ($\sim 20\,000$ people km²; DSEC, 2014). The Macau SAR now consists of the Macau Peninsula (MP) and the Taipa, Cotai, and Coloane (TCC) islands (see Fig. S1 in the Supplement). In particular, the Cotai Reclamation Area is a piece of newly reclaimed land on the top of the bay area between Taipa and Coloane, where new casinos and hotels have been constructed since land of Macau is scarce. Nearly 90% of Macau’s total population is concentrated in the MP, where the population density is significantly higher than the combined density of the Taipa, Cotai, and Coloane (TCC) regions (i.e. 56 000 vs. 6 500, unit in people km⁻²). The MP geographically consists of five regions, nominally parishes. Among those five parishes, the St. Anthony Parish where the ruins of St. Paul’s Cathedral is lo-

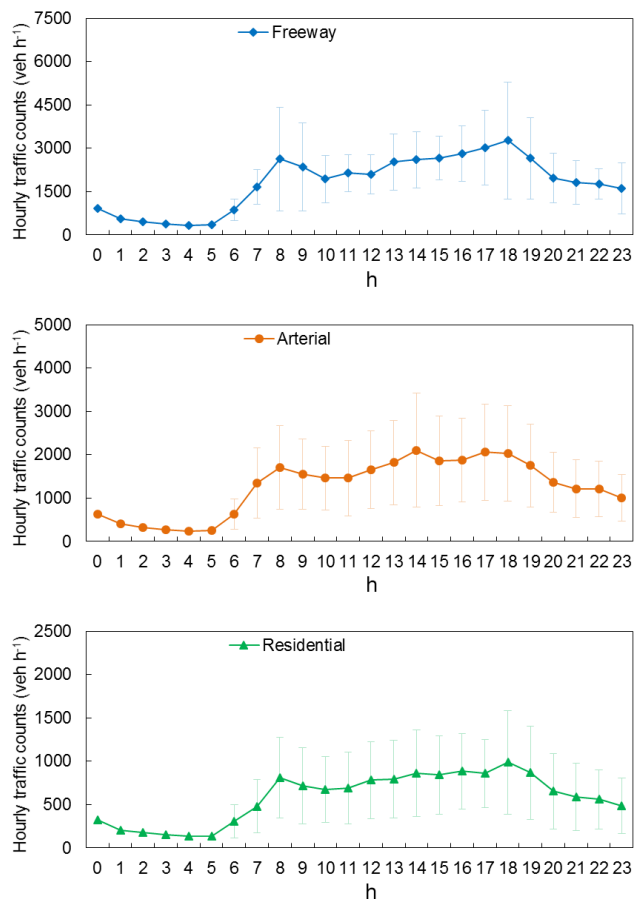


Figure 2. Mean hourly traffic accounts of observed links by road class during weekdays in 2010. The error bars indicate standard deviations of observed data from 06:00 to 23:00

cated has the highest population density, which is approaching $120\,000$ people km^{-2} .

Based on the GIS database of road network in Macau provided by the Macau Transportation Bureau, there were a total of 1704 road links in the study year of 2010. We categorized all those links into three road classes: urban freeways, arterial roads, and residential roads, representing how the level of service decreases from high to low. It should be noted that the road links are unevenly distributed among various areas of Macau, but are similar to the spatial patterns. For example, 77 % of all road links (i.e. 1306 links) were concentrated in the Macau Peninsula, which were responsible for 59 % of Macau's total road length.

2.3 Field investigation and simulation of link-based traffic data

We investigated traffic data on 47 typical road links during over field investigation periods from January 2010 to January 2011 (i.e. nearly 20 weekdays in January 2010, May 2010, and January 2011; see Fig. S2), according to the spa-

tial heterogeneity of road network in Macau by covering all road classes and regions. The length coverage proportion of urban freeways was higher than that for arterial and residential roads, because of higher traffic volumes on the urban freeways. The real traffic flow records of each link was collected with a portable video camera for at least 20 min within each hour. Among all links investigated, five typical road links varying in road classes (one freeway, two arterial roads, and two residential roads) were investigated for the entire day (i.e. 24 h sampling). Sampling duration for the rest of the links investigated were in general from 06:00 to 23:00. (i.e. daytime sampling). Detailed hourly traffic volumes by vehicle classification for 47 road links were further broken down based on those original video profiles by major region and road class (see Table 1). We can clearly observe variations in hourly total traffic counts for three road classes, with significant peaks of traffic demand during morning and evening rush hours (see Fig. 2 and Table 1).

Traffic volume fraction by vehicle classification is another essential type of data obtained from traffic video records (see Fig. S3 as an example of arterial roads). During the evening rush hour (18:00–19:00), LDPVs and MCs, which are the two major vehicle types used for daily commuting in Macau, contributed nearly 80 % of total traffic volume. In particular, MCs are low-cost commuting vehicles for the relatively lower income group in Macau. Therefore, the observed traffic fraction of MCs (~ 45 %) was higher than that of LDPVs (~ 35 %) on the arterial roads of the Macau Peninsula. By contrast, observed traffic fraction of MCs in the TCC was only approximately 15 %. In addition to the spatial variations among various road classes and areas, we also observed temporal variations of various vehicle classifications. Taking arterial roads in the MP, for example, the average traffic fraction of taxis was approximately 10 % during the daytime (06:00 to 12:00). At night-time (12:00 to 06:00), accompanied by significantly reduced traffic demand of MCs and LDPVs, taxis could be responsible for 20–30 % of total vehicle counts. Due to the minor economic contribution of local industry, the average traffic fraction of trucks in Macau indicating freight transportation was significantly lower than those in Beijing and Guangzhou. Furthermore, for the other road links without observed traffic fraction data, we used the hourly and area-aggregated proportions for further modelling (see Eq. 3).

$$\overline{VF}_{a,c,h,v} = \frac{1}{N_{TV_{a,c,h,v}}} \cdot \sum_{l \in (a,c)} VF_{a,c,h,l,v}, \quad (3)$$

where $\overline{VF}_{a,c,h,v}$ is average traffic volume fraction for area a , road class c , hour h , and vehicle classification v ; $N_{TV_{a,c,h,v}}$ is the number of road links with the investigated traffic volume available for area a , road class c , hour h , and vehicle classification v ; $VF_{a,c,h,l,v}$ is the average traffic volume fraction for hour h , road link l , and vehicle classification v , and the link is in area a and under the road class c .

Table 1. Twenty-four hour allocations of total traffic counts by region and road class during weekdays in Macau in 2010.

Region		The Macau Peninsula			The Taipa, Cotai, and Coloane region		
Road classes		Freeway	Arterial	Residential	Freeway	Arterial	Residential
Hour	0	0.021	0.017	0.021	0.021	0.017	0.022
	1	0.013	0.014	0.013	0.013	0.014	0.013
	2	0.011	0.009	0.011	0.011	0.010	0.011
	3	0.009	0.007	0.009	0.009	0.007	0.009
	4	0.008	0.007	0.008	0.008	0.007	0.008
	5	0.008	0.008	0.008	0.008	0.008	0.008
	6	0.021	0.024	0.020	0.021	0.024	0.021
	7	0.029	0.051	0.029	0.029	0.022	0.030
	8	0.051	0.057	0.059	0.048	0.053	0.061
	9	0.048	0.054	0.048	0.042	0.052	0.051
	10	0.044	0.049	0.050	0.046	0.055	0.049
	11	0.055	0.050	0.049	0.056	0.056	0.048
	12	0.051	0.056	0.055	0.051	0.056	0.058
	13	0.059	0.062	0.061	0.062	0.064	0.062
	14	0.060	0.066	0.064	0.070	0.073	0.059
	15	0.064	0.061	0.059	0.068	0.072	0.065
	16	0.066	0.061	0.060	0.071	0.070	0.046
	17	0.066	0.066	0.059	0.065	0.069	0.069
	18	0.071	0.066	0.076	0.062	0.060	0.070
	19	0.061	0.057	0.062	0.054	0.051	0.075
	20	0.049	0.045	0.052	0.049	0.046	0.045
	21	0.048	0.041	0.052	0.048	0.042	0.050
	22	0.047	0.039	0.042	0.047	0.039	0.039
	23	0.042	0.033	0.032	0.042	0.034	0.033

The TransCAD 5.0 model was applied to estimate total traffic demand and its spatial allocation at the link level. TransCAD 5.0, one of the most widely used traffic planning software, can estimate the origin–destination (OD) matrix of the road network from link traffic counts. In this study, we selected the multiple path matrix estimation (MPME) procedure provided by the TransCAD 5.0 and estimated total traffic volumes of all road links during the hour 18:00–19:00 with observed hourly traffic counts of 33 links as input data. After a number of iteration runs, the average discrepancy between simulated traffic volumes and the observed values (i.e. output vs. input) is 4.3 %, and the Pearson coefficient is 0.95, indicating statistically satisfactory results (see Fig. S4). We could identify wide variations in hourly traffic activity among individual roads of one road class group (see Fig. 2), and the variations may be attributed to the difference in the designed traffic capacity (e.g. number of lanes) and location. In terms of the hourly allocation of traffic volume, which is a non-dimensional indicator of temporal variability, the results could indicate good consistency among individual roads with much lower variations (see Fig. S5). Therefore, for other hours, we estimated hourly total traffic volumes based on the averaged temporal allocations and simulated traffic volumes

at 18:00–19:00, as Eq. (4) illustrates.

$$TV_{h,l} = TV_{18,l} \cdot \frac{\bar{\alpha}_{a,c,h}}{\bar{\alpha}_{a,c,18}}, \quad (4)$$

where $TV_{h,l}$ is the hourly total traffic volume for road link l during the hour h , veh h^{-1} , and $TV_{18,l}$ is the hourly data for 18:00–19:00, simulated by the TransCAD if observed traffic volume data are unavailable; $\bar{\alpha}_{a,c,h}$ is the averaged ratio of hourly total traffic volume during the hour h to daily total traffic volume for the area a and the road class c . Therefore, the traffic volumes by vehicle classification are further estimated based on the traffic fraction data averaged by area, road class, and hour. The total 24 h traffic activity by vehicle classification can be estimated with Eq. (5).

$$TA_{\text{daily}_v} = \sum_{h=0}^{23} \sum_l TV_{h,l} \cdot L_l \cdot VF_{h,l,v}, \quad (5)$$

where TA_{daily_v} is the daily traffic activity in the entire research domain for vehicle classification v , veh km d^{-1} ; $VF_{h,l,v}$ is the hourly traffic volume fraction for hour h , link l , and vehicle classification v , and if the $VF_{h,l,v}$ is not available from the traffic field study data, $VF_{h,l,v}$ would be applied by the aggregated data (i.e. $\bar{VF}_{a,c,h,v}, l \in (a, c)$) that is estimated according to Eq. (3).

In addition to traffic volume, traffic condition indicated by link-based hourly speed is another category of essential input data. First, we used a portable GPS receiver to collect second-by-second vehicle trajectory data for on-road vehicles during the same field sampling periods of traffic counts. Considering the distinctions of driving behaviours among MCs, PBs, and other vehicle classifications (e.g. passenger vehicles and trucks), like more frequent stops for PBs to discharge and receive passengers, we used a taxi equipped with the GPS receiver to chase LDPVs randomly to represent traffic conditions for on-road vehicles other than PBs and MCs. Each targeted vehicle was chased for at least 10 m. For PBs and MCs, we selected typical vehicles to record their traffic trajectory data. In this study, we collected traffic trajectory data of LDPVs, PBs, and MCs for 32, 24, and 8.4 h respectively, with high abundance of spatial and temporal distribution. Second, we integrate the original second-by-second GPS trajectory data with the road network GIS system to identify the road link information (e.g. link name, parish, and road class) for each sampling second. Third, we estimated averaged hourly speed for each road class in each parish.

$$\bar{V}_{a,c,h,v} = \frac{1}{N_{V_{a,c,h,v}}} \cdot \sum_{l \in (a,c)} \bar{V}_{a,c,h,l,v}, \quad (6)$$

where $\bar{V}_{a,c,h,v}$ is average hourly speed for road class c , hour h , region r , and vehicle classification v (LDPVs, PBs, and MCs in this equation), km h^{-1} ; $N_{V_{a,c,h,v}}$ is the number of link with the investigated speed available for road class c , hour h , area a , and vehicle classification v ; $\bar{V}_{a,c,h,l,v}$ is the average speed for hour h , road link l , and vehicle classification v , km h^{-1} , and the link is in area a and under the road class c . Considerable temporal and spatial variability in the hourly speeds across road links remained due to the limited data compared with the vast entire road network. For example, the coefficients of variation for the hourly speeds of arterial roads in the MP were 48, 40, and 48 % respectively, during a morning rush hour (14 road samples, 08:00), a noon-time hour (16 road samples, 12:00), and an evening rush hour (13 road samples, 18:00) within a single investigation day. In other cities or regions where intelligent transportation systems (ITS) are developed, we suggest the application of ITS-informed traffic data to better capture the temporal and spatial traffic heterogeneity among various road links.

To validate the speed profiles, we observed variations in average hourly speeds by area and road class for LDPVs as an example, which were aggregated by link-level speed profiles with traffic volume data taken into account (see Fig. 3). Clearly, average hourly speeds for arterial and residential roads in the MP were lower than 20 km h^{-1} for longer than 15 h (e.g. from 06:00 to 20:00), indicating extremely congested traffic conditions. In particular, average hourly speeds during the evening rush-hour period (e.g. 18:00–19:00) were even less than 15 km h^{-1} , which corresponded to the officially released data. In the TCC, where traffic is less popu-

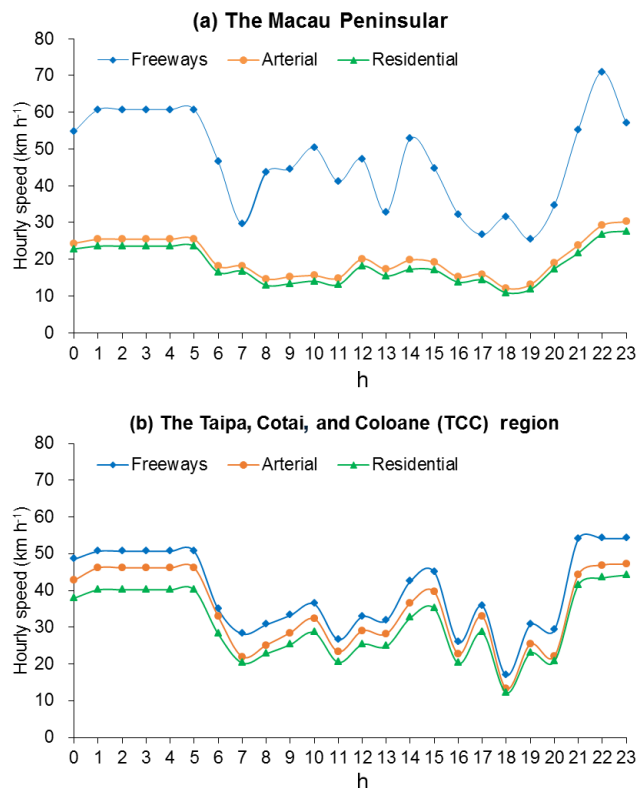


Figure 3. Variations in aggregated hourly speeds by road class and region for LDPVs during weekdays in 2010.

lated, average hourly speeds for arterial and residential roads were significantly higher than those in the Macau Peninsula, ranging from 20 to 40 km h^{-1} except for the hour 18:00–19:00. On the other hand, we could also observe differences of aggregated daily speed among various vehicle classifications (see Fig. S6). For example, average daily speed of taxis was 24.0 km h^{-1} , higher than the 21.7 km h^{-1} of LDPVs, due to higher traffic volume fraction of taxis at night-time when there were usually free traffic flows. Similarly, the average speed of HDTs was 27.0 km h^{-1} , topping all vehicle classifications, because their traffic volume fraction was significantly higher in the TCC compared to the MP.

2.4 Emission factor development and the integration with traffic data and vehicle age distribution

We initiated a comprehensive measurement programme of collecting real-world emission profiles since 2010 in order to establish and update a localized emission factor model for vehicles in Macau (e.g. the the emission factor model for the Beijing vehicle fleet – Macau, EMBEV–Macau model). So far, more than 60 typical vehicles, LDPVs, taxis, PBs, LDTs, and HDTs, have been measured on road by using a portable emission measurement system (PEMS). Furthermore, a large-scale remote sensing vehicle emission measurement project was conducted in March and April 2008,

which enabled the collection of fuel-based emission factors for MCs in Macau. A detailed experimental section for Macau and the measurement results are documented in several of our previous papers regarding gasoline, diesel, and more advanced vehicles (e.g. hybrid electric vehicles; Hu et al., 2012; Wang et al., 2014; Zhang et al., 2014b, d; Zhou et al., 2014; Wu et al., 2015a, b; Zheng et al., 2015, 2016). We developed an emission factor model, the EMBEV-Macau model, with reference to the modelling framework and methodology of the EMBEV model, which is originally developed for the vehicle fleet in Beijing (Zhang et al., 2014a). Technically, these two emission measurement methods (PEMS and remote sensing) have their own useful features and practical limitations for developing emission factors. As for the PEMS testing, it can provide accurate measurements of real-world emissions for an entire trip for each vehicle. However, the PEMS method usually collects limited vehicle samples due to the expensive and time-consuming experimental process. In contrast, the remote sensing method could collect large-sized vehicle samples so it is capable of presenting the emission trends over a wide spectrum of model years and vehicle conditions (Zhou et al., 2014; Bishop et al., 2012). However, the short test duration and limited test sites of remote sensing measurements are also questioned for the representativeness of vehicle emissions (Lee and Frey, 2012; Chen and Borken-Kleefeld, 2015). Thus, we attempted to use the advantage of each measurement method to develop local emission factors. Taking the gasoline LDPVs, for example, the remote sensing results indicated that vehicles with model year (MY) later than 2004 have consistently lower gaseous emissions (Zhou et al., 2014), which were comparable to those of modern vehicles complying with the Euro 5 emission standard (Zhang et al., 2014a). We assumed these post-MY 2004 gasoline LDPVs are one vehicle age group, and apply the basic emission parameters of the Euro 5 for the post-MY 2004 gasoline LDPVs in Macau (e.g. basic emission factors, deterioration rates) with additional modifications. First, we developed localized speed correction curves based on a microtrip method for each vehicle classification to integrate vehicle emission factors and traffic conditions at the link level (Zhang et al., 2014b, c; Wu et al., 2015b). Second, we used the PEMS results to derive the extra emissions in the start stage, and modified the start emission parameters (e.g. gram per start). Third, the EMBEV-Macau model enables us to correct impacts of local temperature, fuel quality, air conditioning usage, and other aspects to the real conditions. For example, the sulfur contents of gasoline and diesel were approximately 90 and 15 ppm in 2010. In addition, the original EMBEV model has already developed detailed distribution functions of emission factors, which can address the effect of high emitters. It is noted that several vehicle fleets have limited PEMS or dynamometer test data in China (e.g. MC). We developed their emission factors mainly based on the remote sensing results (Zhou et al., 2014).

Considering that there was no significant policy influencing traffic flow composition during the years 2008–2010, we estimated detailed traffic fraction by fuel type and vehicle age for each vehicle classification based on the vehicle information database from the 2008 remote sensing project (Zhou et al., 2014). It should be noted that some vehicle classifications have a single fuel type, e.g. gasoline for MCs and diesel for PBs. By contrast, other vehicle specifications like engine displacement have a more important effect on real-world emissions. Therefore, we also derived the on-road traffic volume split ratios by engine displacement for MCs and PBs (refer to the footnote of Table 2). Table 2 illustrates the detailed traffic volume fraction by vehicle age and fuel type (or split by engine displacement for MCs and PBs) for each vehicle classification.

2.5 Modelling dispersion of vehicular air pollutants

Urban air quality models are commonly used to estimate the spatial distribution of vehicular pollutants by simulating their chemical and physical processes in the atmosphere within urban areas. Holmes and Morawska (2006) classified dispersion models into box models, Gaussian models, Lagrangian models, and computational fluid dynamic (CFD) models. Currently, Gaussian models are recommended by the environmental protection agencies of most countries all over the world.

The AMS/EPA regulatory model (AERMOD) is a steady-state Gaussian plume dispersion model which is recommended by US EPA (US EPA, 2004). The modelling system consists of one main programme (AERMOD) and two pre-processors (i.e. AERMET and AERMAP). In addition, calculating urban boundary layer parameters and considering urban heat island effects makes AERMOD sensitive to local meteorological conditions. Recently, several studies have investigated the integration performances of the traffic simulation model, vehicle emission model, and the AERMOD model. For example, Vallamsundar and Lin (2012) integrated MOVES (Motor Vehicle Emissions Simulator) and AERMOD models to simulate the PM_{2.5} hotspot cases of typical roads in US cities (i.e. study domain area of $\sim 0.5 \text{ km}^2$) and provided some implications based on sensitivity analysis, such as narrowing the data gap between traffic, emissions, and air quality models and further investigation of important local input data (e.g. traffic composition, fleet age distribution). Misra et al. (2013) also integrated a traffic simulation model, a vehicle emission model, and the AERMOD model to estimate traffic-related pollution in downtown Toronto (i.e. study domain area of $\sim 0.5 \text{ km}^2$). It should be noted that, in those previous investigations at near-field level (Zannetti, 1990), the AERMOD simulated vehicular emissions as a series of point sources which approximate a traffic lane.

Considering a significantly larger study area, higher road density, and the scarcity of metrological data and surrounding building profiles at a sufficiently fine resolution, we

Table 2. Summary of age allocation for on-road fleets by vehicle classification in Macau.

Vehicle classification	LDPV		MC		Taxi	PB		MDPV		HDPV	LDT		HDT	
Subclassification	G ^a	D ^b	Heavy ^c	Light ^c	D	Medium ^d	Heavy ^d	G	D	D	G	D	D	
Ratio	0.99	0.01	0.68	0.32	1.00	0.33	0.67	0.53	0.47	1.00	0.25	0.75	1.00	
Vehicle age	1	0.12	0.12	0.18	0.09	0.14	0.00	0.08	0.20	0.16	0.20	0.12	0.08	0.02
	2	0.10	0.17	0.15	0.08	0.13	0.00	0.08	0.17	0.17	0.06	0.17	0.18	0.15
	3	0.10	0.08	0.19	0.09	0.04	0.00	0.08	0.07	0.12	0.09	0.11	0.10	0.11
	4	0.10	0.11	0.14	0.07	0.06	0.00	0.18	0.06	0.02	0.10	0.03	0.09	0.04
	5	0.09	0.03	0.08	0.04	0.06	0.17	0.16	0.05	0.09	0.09	0.03	0.05	0.03
	6	0.06	0.05	0.05	0.07	0.02	0.12	0.14	0.05	0.03	0.09	0.09	0.04	0.01
	7	0.05	0.01	0.04	0.04	0.11	0.25	0.15	0.06	0.01	0.03	0.00	0.02	0.01
	8	0.05	0.02	0.04	0.07	0.16	0.05	0.05	0.08	0.01	0.05	0.05	0.02	0.00
	9	0.04	0.03	0.02	0.08	0.24	0.00	0.00	0.04	0.01	0.05	0.02	0.02	0.01
	10	0.04	0.06	0.01	0.13	0.01	0.07	0.00	0.06	0.02	0.04	0.01	0.03	0.02
	11	0.05	0.06	0.03	0.14	0.03	0.17	0.01	0.02	0.01	0.10	0.02	0.04	0.01
	12	0.05	0.04	0.02	0.06	0.00	0.00	0.03	0.03	0.01	0.04	0.01	0.04	0.02
	13	0.03	0.06	0.00	0.01	0.00	0.03	0.00	0.02	0.03	0.00	0.02	0.02	0.01
	14	0.04	0.05	0.01	0.01	0.00	0.10	0.00	0.02	0.03	0.00	0.06	0.04	0.04
	15	0.03	0.05	0.01	0.01	0.00	0.05	0.00	0.04	0.05	0.00	0.06	0.04	0.11
	16	0.02	0.02	0.01	0.00	0.00	0.00	0.00	0.03	0.04	0.03	0.04	0.06	0.16
	17	0.01	0.03	0.00	0.01	0.00	0.00	0.00	0.00	0.03	0.00	0.05	0.04	0.06
	18	0.01	0.01	0.00	0.00	0.00	0.00	0.00	0.00	0.06	0.00	0.05	0.03	0.03
	19	0.00	0.00	0.00	0.00	0.00	0.00	0.04	0.00	0.02	0.00	0.02	0.02	0.07
	20	0.00	0.01	0.00	0.00	0.00	0.00	0.00	0.00	0.07	0.02	0.03	0.05	0.08
Fleet-average vehicle age	6.7	7.3	4.4	7.2	5.8	8.6	5.5	5.7	7.9	6.0	8.1	8.1	11.4	

^a Gasoline; ^b diesel; ^c breaking point of engine displacement 50 mL; ^d breaking point of engine displacement at 5.0 L.

divided the study domain into a grid of 350 square cells (500 m × 500 m). Aggregated hourly vehicular emissions of major pollutants (e.g. CO and PM_{2.5}) from all road links in each grid are used as the input data for the AERMOD. The receptors are placed at the central points of all cells at a height of 2.0 m. In terms of the geographic data and the altitude, information is obtained from Google Earth. Building downwash effects are simulated by the AERMOD. In our study, we model the weekdays of November 2010 when rainy days were much fewer compared to other months. Hourly meteorological profiles from two monitoring sites located in MP and TCC respectively, including temperature, wind direction, wind speed, relative humidity, and air pressure, are provided by the Department of Metrological Services in Macau. The north-easterly winds are prevailing during that month, supplemented by a minor part of northerly and easterly winds (see Fig. S7).

It is noted that the AERMOD has the function of simulating the dispersion of NO_x as well as the oxidation process from freshly emitted NO to ambient NO₂ with simplified chemical mechanisms (US EPA, 2015). For example, the AERMOD considers NO conversion to NO₂ by reaction with ambient ozone (i.e. NO + O₃ → NO₂ + O₂, which is used by both two EPA Tier 3 methods such as OLM (Ozone Limiting Method) and PVMRM (Plume Volume Molar Ratio Method); US EPA, 2015; Podrez, 2015). However, the NO/NO₂ conversion module of the AERMOD is developed

based on simplified mechanism and regressions using historical monitoring data, which may have several limitations compared to actual complex chemistry. First, there are numerous other reactions that would further oxidize NO₂ to other NO_y species (e.g. nitrate radical, nitrate acid, peroxyacyl nitrates), and Pollack et al. (2012) suggest that the production of these NO_y species may differ by period (e.g. daytime vs. night-time; weekdays vs. weekends). However, these reactions removing NO₂ from the atmosphere have not been considered by the AERMOD. Second, this basic chemical reaction in the AERMOD (NO + O₃ → NO₂ + O₂) is simply assumed to be instantaneous and irreversible on an hourly basis (US EPA, 2015). The convention ratio is greatly dependent on the ambient ozone concentration (both OLM and PVMRM) and the estimated mixing status of ambient ozone in the plume (PVMRM). However, the spatial distribution of ambient ozone concentration in a city is highly heterogeneous (Murphy et al., 2007), which is a substantial hurdle to assure the simulation accuracy over a city-level area. For these reasons, we did not include the NO₂ simulation results in the paper and accordingly have a discussion on this issue in a later section.

Table 3. Spatially explicit estimation of traffic counts in Macau.

Region	Daily traffic counts by road class (10^5 veh)			Hour-based density of traffic volume (10^4 veh h^{-1} km $^{-2}$)	
	Freeway	Arterial	Residential	Daily average	Evening rush hour (18:00)
Macau Peninsula	15.2	70.8	138.4	10.0	17.3
Saint Antony Parish	2.8	20.5	35.0	25.3	44.3
Taipa, Cotai, and Coloane	6.9	13.9	28.8	1.0	1.5
Taipa	2.2	12.5	17.8	2.0	3.1
Cotai	3.6	1.4	7.1	0.8	1.3
Coloane	1.1		3.9	0.3	0.5
Total	22.2	84.7	170.2	3.8	6.5

3 Results and discussion

3.1 Estimated traffic activity and vehicle emissions

Table 3 presents spatially explicit traffic counts during a typical weekday and an evening rush hour (i.e. 18:00) respectively. More than 80 % of total daily traffic counts were concentrated in the MP, 160 % higher than the overall average of Macau. In particular, the Saint Antony Parish with an internationally renowned tourist attraction (e.g. the ruins of St. Paul's) had a top hour-based density of daily traffic volume as a result of its substantial population density. Furthermore, traffic activity (unit veh km h^{-1} or veh km d^{-1}) can be estimated as the product of traffic counts and link length, namely $TV_{h,l,v}$ and L_l (see Eq. 1), which is an essential indicator of vehicle-use intensity. Estimated daily traffic activity of Macau's total vehicles in a typical weekday of 2010 is 4.04×10^6 veh km d^{-1} (see Table S1 in the Supplement). LDPVs and MCs rank first and second among all vehicle classifications, accounting for 43 and 30 % of total daily traffic activity in Macau. Therefore, fleet-average daily vehicle kilometres travelled (VKT) of LDPVs and MCs during weekdays in 2010 are 20.8 and 11.7 km respectively. If we ignore the potential difference between weekdays and weekends, fleet-average annual VKT of LDPVs and MCs registered in Macau are 7600 and 4300 km as of 2010, which are quite comparable with our previous survey results. Those values could only be responsible for traffic demand within Macau, considering a part of LDPVs travel across the boundary of the Macau SAR into mainland China. It is worth noting that the annual VKT of LDPVs registered in Macau is significantly lower than those of Beijing and Guangzhou (Zhang et al., 2013, 2014a). The major reason is that the scale of Macau is much smaller than the megacities of mainland China (e.g. Beijing, Guangzhou), approximately 15 km from the northernmost parish in MP to Coloane Island. Since fewer MCs drive on the cross-sea bridges, a major part of MCs' traffic activity (note: in particular for light-duty two-stroke MCs) is largely limited within MP or TCC. Therefore, the traffic

activity of MCs is lower than LDPVs but with higher traffic counts, which have an estimated annual VKT comparable to the value in mainland China (e.g. 5000–6000 km; Zhang et al., 2013, 2014a).

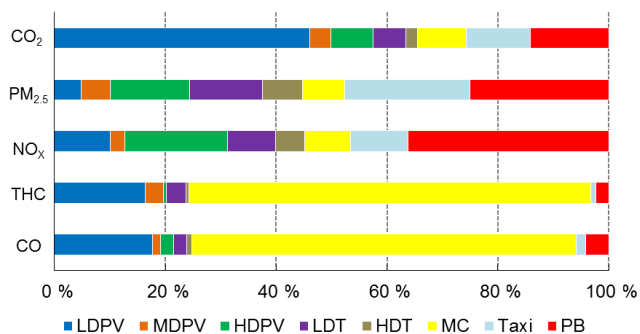
Table 4 presents estimated average distance-specific emission factors of major air pollutants by vehicle classification and fuel type for a typical weekday in Macau during 2010. Average CO and THC emission factors for gasoline-powered LDPVs in Macau are significantly lower by 57 and 30 % respectively, compared to those of gasoline LDPVs registered in Beijing, although the average driving speed of LDPVs in Macau is lower than in Beijing (e.g. ~ 22 km h^{-1} vs. 30 km h^{-1}). A major reason for this estimation is that a majority of the gasoline cars are imported from Japan, where vehicle emission standards are in general more stringent than those implemented in mainland China (Wang et al., 2014). By contrast, compared to gasoline taxis in Beijing, diesel engines in the taxi fleet in Macau led to significantly higher NO_x and $PM_{2.5}$ emission factors of 3.5 and 17 times (Hu et al., 2012; Zhang et al., 2014a). For heavy-duty diesel trucks and buses, lower speed and a higher proportion of older vehicles resulted in higher NO_x and $PM_{2.5}$ emission factors in Macau than in Beijing. For MCs, in particular light-duty two-stroke MCs, their fleet-average THC emission factors are significantly higher than for other vehicle technology types (Zhou et al., 2014).

Estimated total vehicular emissions in a typical weekday during 2010 are 16.8 t of CO, 3.58 tons of THC, 5.00 tons of NO_x , and 0.28 tons of $PM_{2.5}$. As Fig. 4 illustrates, emission allocation patterns by vehicle classification are different for various pollutant categories. Compared to well-controlled CO and THC emission factors of LDPVs, MCs are estimated to have been responsible for 69 and 72 % of total vehicular emissions for CO and THC respectively. In particular, two-stroke MCs contribute 45 % of total THC vehicular emissions, which led the Macau government to initiate a replacement of two-stroke MCs with small-size four-stroke MCs after 2010. Furthermore, a possible promotion of electric MCs in Macau is also under consideration by policy makers in

Table 4. Estimated fleet-average emission factors under real-world driving conditions.

Vehicle classification	Fleet-average emission factors (g km^{-1})					Emission measurement data sources
	CO	THC	NO_x	$\text{PM}_{2.5}$	CO_2	
LDPV-gasoline	1.74	0.34	0.28	0.006	263	PEMS ^a , RS ^b , EMBEV ^c
MDPV-gasoline	2.80	1.78	1.03	0.030	379	RS
MDPV-diesel	1.60	0.27	1.44	0.26	307	RS, EMBEV
HDPV-diesel	4.76	0.25	10.9	0.48	914	RS, EMBEV
LDT-gasoline	6.36	1.75	0.61	0.014	250	RS
LDT-diesel	1.69	0.65	4.03	0.35	485	PEMS, RS, EMBEV
HDT-diesel	7.40	0.94	12.3	0.95	1010	PEMS, RS, EMBEV
Taxi	0.47	0.06	0.86	0.11	192	PEMS, RS
MC-light	7.95	4.07	0.26	0.030	39	RS
MC-heavy	10.2	1.18	0.38	0.012	86	RS
PB-medium	2.45	1.09	6.50	0.32	555	PEMS, RS, EMBEV
PB-heavy	6.05	0.35	15.8	0.57	1215	PEMS, RS, EMBEV

^a PEMS measurement data in Macau; ^b remote sensing data in Macau; ^c dynamometer or PEMS measurement data of sufficient vehicle samples involved in the original EMBEV model (Zhang et al., 2014a).

**Figure 4.** Allocations of total vehicular emissions by vehicle classification.

Macau. For both NO_x and $\text{PM}_{2.5}$, diesel-powered passenger fleets contributed 60–65 % of total vehicular emissions, including PBs, taxis, and HDPVs mainly owned by hotels and casinos. By contrast, diesel trucks contributed approximately 15 to 20 % of total NO_x and $\text{PM}_{2.5}$ emissions in Macau, substantially lower than the contribution of diesel trucks registered in other populated cities of China (e.g. 30–35 % for Beijing and Guangzhou; Zhang et al., 2013, 2014a). This phenomenon should be attributed to the significantly higher passenger transportation demand than freight transportation in Macau, as tourism and the entertainment industry are the pillars of the local economy. Our results clearly suggest that policy makers in Macau should carefully focus on various vehicle classifications when facing emission mitigation targets for various air pollutants.

For CO_2 emissions, unfavourable operating conditions like lower driving speeds and frequent use of air conditioning systems resulted in substantial climate and energy penalties for passenger vehicles (e.g. LDPVs, taxis, PBs). For example, the estimated average CO_2 emission factor of LDPVs is

263 g km^{-1} (see Table 4), a significant increase of approximately 25 % compared to on-road measurement results under a higher average speed ($205\text{--}210 \text{ g km}^{-1}$ at 30 km h^{-1}). This is equivalent to $\sim 13 \text{ L}$ per 100 km fuel consumption, indicating a substantial increase of CO_2 and fuel consumption under real-world driving conditions than those measured under the type-approval conditions applied in current regulatory systems (e.g. both Japan and Europe). Overall, the estimated total CO_2 emissions from all vehicle classifications and all road links are 1001 tons during a typical day. LDPVs, PBs, and taxis are estimated to have been responsible for 46, 14, and 12 % of total daily CO_2 emissions respectively (see Fig. 4), ranking in the top three among all classifications.

Our previous evaluation indicates estimated macro uncertainty (i.e. annual emission inventory by using registration data) for air pollutants (e.g. CO, THC, NO_x , and $\text{PM}_{2.5}$) is approximately $-30 \%/+50 \%$ at a 95 % confidence level (Zhang et al., 2014a). The skewed probability distribution is due to high emitters of air pollutants within the fleet. The uncertainty in CO_2 emissions would be narrower due to detailed localized vehicle information, and fuel economy data are used in estimation, plus they are strongly corrected for average speed. It is noted that the Macau SAR is a relatively closed island city with special border controls (e.g. road transport to mainland China). Only the vehicles issued with special licence plates in the Macau SAR and Guangdong province (i.e. two licence plates) can be driven across the border. This circumstance offers an opportunity to validate the gasoline fuel CO_2 emissions with the statistical fuel consumption record, since almost all the gasoline fuels are consumed by on-road vehicles in Macau. Our emission inventory estimated that total gasoline consumption by on-road vehicles in Macau would be 180 t during a typical weekday of 2010 (note: the carbon mass fraction is assumed 0.87). If using this value as the daily average for 365 days of a year, to-

tal gasoline consumption would be 65.7 kt in 2010, compared to a statistical consumption amount of 81 700 m³ (approximately 60 kt). The relative bias is within a reasonably narrow range ($\sim 10\%$) and can be attributed to two major reasons. First, the yearly estimation of gasoline consumption (65.7 kt) assumed the same vehicle activity on weekdays and at weekends. The vehicle activity on weekends might be less than that on weekdays due to the absent commuting demand. Second, the gasoline price in Guangdong province was lower by approximately 20% than Macau during 2010, which could be an important incentive for the users of those LDPVs with two licence plates to choose to refill their vehicles in Guangdong while using them in Macau. For the diesel sector, the statistical data do not specify the amount consumed by on-road vehicles, and non-road engines would contribute substantially to the total diesel use in Macau. We suggest further validation be conducted if the on-road diesel consumption amount is available, since diesel vehicles could considerably account for total NO_x and PM_{2.5} emission even if their traffic fractions are at a low level (Dallmann et al., 2013). We could address the uncertainty in link-level vehicle emissions with the big traffic data (see the discussion in the next subsection) available for typical roads in the future.

3.2 Temporal and spatial variations in traffic-related emissions

High strong correlations between temporal variations in traffic activity and emissions are clearly observed for all air pollutants and CO₂ ($R^2 > 0.92$, see Fig. 5). For example, the 18:00–19:00 hour contributed 6.9% of total daily traffic activity, when hourly emissions of gaseous species (CO, THC, NO_x and CO₂) were responsible for 7.9–8.7% of their daily emissions. This was because emission factors of gaseous pollutants and CO₂ increased during the rush hours due to lower driving speed. The increases were 15–26% for their emission factors compared to the daily averages. Compared with night-time, average gaseous emission factors of the total fleet increased by 51–120%. The elevation of PM_{2.5} emissions in the rush hour was not as significant as gaseous species, because the traffic demand of diesel fleets (e.g. HDPVs, taxis, PBs, trucks) increased less relative to gasoline fleets (e.g. MCs, LDPVs) in Macau.

Spatial distributions of vehicular emissions are associated with real-world traffic characteristics including total traffic counts, traffic conditions, and fleet composition. To sum up, 58% of NO_x, 52% of PM_{2.5}, and 59% of CO₂ vehicular emissions were estimated from the road network of the MP (see Fig. 6 for NO_x, Fig. S8 for other pollutants and Table S2 for the summary of spatial distribution). Meanwhile, 76% of CO and 78% of THC emissions were aggregated from on-road vehicles within the MP. The discrepancy of emission spatial allocations between CO/THC and NO_x/PM_{2.5}/CO₂ is primarily because of the higher fleet penetration of MCs in the MP. That is to say, relative inaccuracy associated with

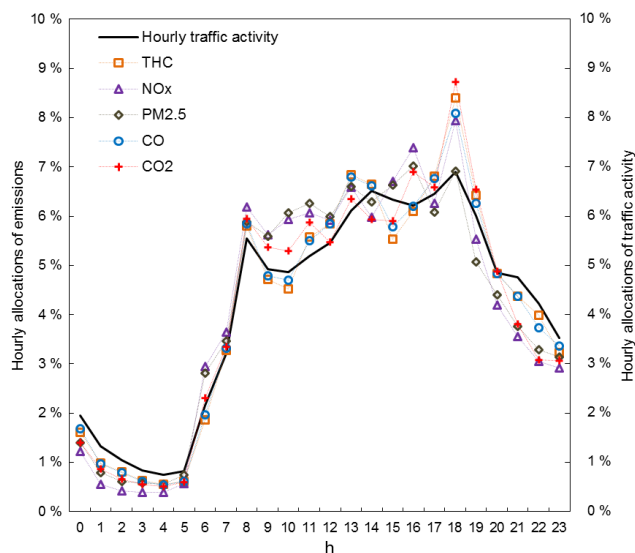


Figure 5. Hourly allocations of vehicular emissions and traffic activity in Macau during weekdays in 2010.

emission spatial allocation by the top-down approach could be up to 20% if real-world fleet composition information is not taken into account. By contrast, the spatial allocations of NO_x, PM_{2.5} and CO₂ at three cross-sea bridges were estimated to be higher by approximately 55–110% than CO and THC, because the traffic volume fraction of MCs was significantly lower than in other regions, in particular compared with the MP.

Detailed statistical profiles of spatial-related vehicular emission are summarized by length-specific emission intensity of road groups and area-specific emission intensity of gridded cells (see Tables 5 and 6). Higher length-specific emission intensities of CO and THC are unexpectedly identified on arterial roads in the MP with fewer traffic accounts compared with their urban freeway counterparts, owing to higher traffic activity of MCs and more severe traffic congestion increasing all-fleet emission factors. For NO_x, PM_{2.5}, and CO₂, higher length-specific emission intensities are all associated with higher level of service for the three road classes, both in the MP and the TCC. Area-specific emission intensities of all pollutants and CO₂ had decreasing trends from north to south (i.e. from the MP to the Coloane Island), similar to the patterns of road density and traffic demand. Emission hotspots are identified in traffic-populated cells of the MP, e.g. the region close the ruins of St. Paul's, where daily area-specific emission intensity of NO_x was as high as 600 kg km⁻² d⁻¹. This level is ~ 4 times that in the whole of Macau and ~ 40 times the level on Coloane Island. Not surprisingly, significant near-field air pollution problems in MP are caused by those extremely higher vehicular emissions due to higher traffic activity density and more significant traffic congestion.

Table 5. Length-specific emission intensity of total vehicular emissions during a typical weekday of 2010.

Region	Road class	Length-specific emission intensity ($\text{kg km}^{-1} \text{d}^{-1}$)				
		CO	THC	NO _x	PM _{2.5}	CO ₂
Macau Peninsula	Freeway	141	28	43	2.6	9.05×10^3
	Arterial	195	42	39	1.9	7.82×10^3
	Residential	79	17	18	0.9	3.74×10^3
Taipa, Cotai, and Coloane	Freeway	73	12	41	2.9	7.41×10^3
	Arterial	54	9	35	2.3	595×10^3
	Residential	24	5	6	0.4	1.91×10^3
Cross-sea bridges	Freeways	109	22	59	4.0	10.8×10^3
Total	Freeway	106	20	48	3.1	9.07×10^3
	Arterial	122	25	38	2.1	6.85×10^3
	Residential	59	13	14	0.7	3.08×10^3

Table 6. Area-specific emission intensity of total vehicular emissions during a typical weekday in 2010.

Region/parish	Area-specific emission intensity ($\text{kg km}^{-2} \text{d}^{-1}$)				
	CO	THC	NO _x	PM _{2.5}	CO ₂
Macau Peninsula	1368	297	312	15.5	6.37×10^4
St. Lazarus Parish	3118	681	695	33.7	12.9×10^4
St. Lawrence Parish	1407	303	305	15.4	6.13×10^4
Our Lady Fatima Parish	1241	271	274	13.7	5.74×10^4
St. Anthony Parish	2485	546	556	26.4	11.8×10^4
Cathedral Parish	784	166	199	10.4	3.86×10^4
Taipa	287	52	150	9.50	2.80×10^4
Cotai Reclamation Area	155	27	70	4.67	1.41×10^4
Coloane	50	10	15	0.88	0.44×10^4
Total land area of Macau	566	120	168	9.42	3.37×10^4

It should be noted that the increasingly broad application of an intelligent traffic system (ITS) and smart vehicle technologies can play a significant role in improving our understanding of dynamic traffic flows, namely enabling the big data collection regarding total traffic volume, fleet composition, and traffic conditions (e.g. speed). For example, the traffic loop detector (TLD) and the vehicle licence plate recognition (VLPR) are both widely used, and economic ITS technologies that began in the early 2000s in China are integrated to provide category-informed vehicle volume, on which many cities in China (e.g. Beijing, Guangzhou) depend to release official data, including year-by-year variations in total urban traffic demand (BJTRC, 2013; Zhang et al., 2013). The traffic loop detector is able to provide vehicle passing speed; however, it is often criticized due to the limited coverage for entire trips or the entire traffic network. The floating car system, namely using the taxi fleet as probe vehicles based on GPS technology, is an advanced moni-

toring tool for real-time traffic conditions. Taking Beijing, for example, its floating car system is capable of mapping link-based traffic conditions for the urban area ($\sim 1000 \text{ km}^2$) every 5 min based on 66 000 taxis and mesh urban average speed layer down at a link level. During 2012, 24 h average speeds of the urban area of Beijing were estimated at $23.2 \pm 2.3 \text{ km h}^{-1}$ for weekdays and $26.9 \pm 3.9 \text{ km h}^{-1}$ for weekends and holidays respectively (BJTRC, 2014; Zhang et al., 2014a, b). Therefore, daily variations in traffic conditions could result in a coefficient of variation (i.e. the ratio of standard deviation to mean value) of 6 % for the distance-specific CO₂ emission factor all year around in Beijing. The speed correction applied for this variation estimation is also applicable to the Macau's road network. If the evaluation level is refined into a link level, the variability and uncertainty in vehicle emissions would be greater due to traffic flows becoming inherently greater as the spatial resolution is enhanced. For example, the variations in hourly speeds of

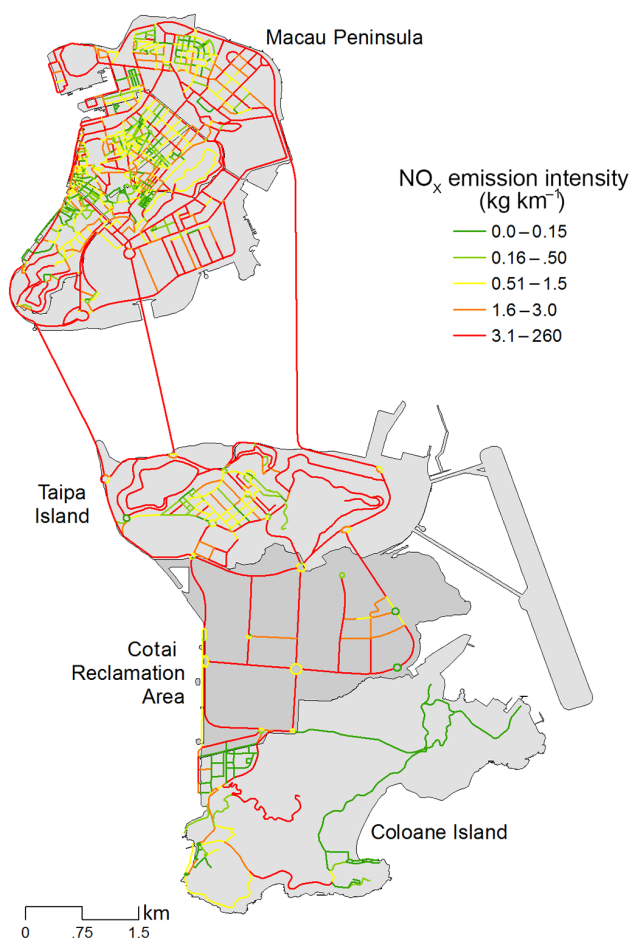


Figure 6. The spatial distribution of NO_x emission intensity for on-road vehicles in Macau on a typical weekday in 2010.

arterial roads in the MP could lead to variations (e.g. 1 standard deviation, 40 % at noontime and 48 % in the rush hours) in fleet-average CO_2 emission factors of gasoline LDPVs of approximately -20 to 45 % during the noontime and -25 to 60 % during rush hours relative to the average CO_2 emission factor levels. In terms of total vehicle emissions, it would be further complicated since the traffic volume is inherently associated with the level of service (e.g. speed) in reality. Most recently, the radio frequently identification (RFID) technology has been applied in a few Chinese cities (e.g. Nanjing, the capital city of Jiangsu province) to provide more accurate vehicle recognition with detailed specifications (e.g. category, fuel type, emission standard, model year, and vehicle size) than the TLD and VLPR. The RFID data in Nanjing are further connected with a smartphone application, based on which more capabilities like environmentally constrained traffic management (e.g. low emission zone, congestion fee programme) could be developed in the future. From the perspective of vehicles, for instance, more real vehicle data can be accessed through the on-board diagnostic (OBD)

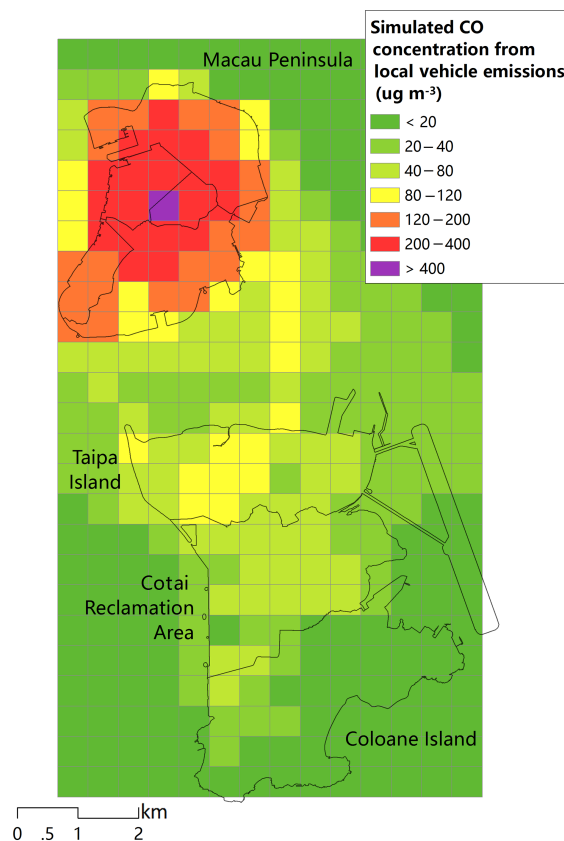


Figure 7. Simulated vehicle-contributed concentration of CO in Macau during weekdays in November 2010.

decoders. The second-by-second data of driving conditions (e.g. speed, acceleration) are able to be combined with an operating mode-based (e.g. VSP-informed) emission model to provide finer emission estimations. While foregoing advanced traffic data collection methods (e.g. TLD, RFID, taxi, fleet-based floating car system) are not available in Macau, the framework of this study is technically feasible in large cities in China where big traffic data are adequately available.

3.3 Simulated concentrations of primary traffic-related pollutants in Macau

Figure 7 presents a spatial map of average concentrations of primary vehicle-contributed CO (see $\text{PM}_{2.5}$ in Fig. S9), which shows the simulated results of all receptors (i.e. central points of cells) with the AERMOD model. The spatial variations in simulated concentrations highly resemble the patterns of area-specific emission intensity for vehicular pollutants. For example, average concentrations contributed by local vehicular emissions in Macau were $86.1 \pm 89.4 \mu\text{g m}^{-3}$ of CO and $1.30 \pm 0.91 \mu\text{g m}^{-3}$ of $\text{PM}_{2.5}$ (see Table 7). Highest receptor concentrations of CO and $\text{PM}_{2.5}$ are 415 and

Table 7. Simulated average contributions contributed by primarily vehicular emissions in Macau, weekdays during November 2010.

Region/parish	Simulated concentrations of primary vehicular emissions ($\mu\text{g m}^{-3}$)					
	CO			PM _{2.5}		
	Mean	Min	Max	Mean	Min	Max
Macau Peninsula	199	57.8	415	2.03	0.67	3.89
St. Lazarus Parish	330	270	415	3.14	2.59	3.89
St. Lawrence Parish	180	139	265	1.72	1.32	2.47
Our Lady Fatima Parish	171	77.8	209	1.64	0.67	3.21
St. Anthony Parish	296	223	362	2.85	2.17	3.39
Cathedral Parish	166	57.8	370	2.03	1.00	3.14
Taipa	42.1	12.6	104	1.65	0.61	2.46
Cotai Reclamation Area	37.1	11.2	63.1	1.08	0.27	2.39
Coloane	16.9	7.0	54.1	0.29	0.12	0.63
Total land area of Macau	84.5	7.0	415	1.30	0.12	3.89

Note: Simulated results for 6–8 November are not accounted in this table due to the impact of rainfall. Mean, minimum, and maximum values are for simulated average concentrations of each receptors in each region/parish during the study period.

$4.42 \mu\text{g m}^{-3}$ respectively, all occurring at traffic-populated cells in the MP.

We further compared modelled concentrations of primary pollutants from local vehicles and official air quality data. Traffic contributions at the monitoring sites are approximated by simulated results for their closest receptors so as to estimate monthly average source proportions of on-road vehicles in Macau. Therefore, source proportions vary from pollutant categories and locations during the time framework of this study. For example, estimated proportions of vehicular CO emissions are $\sim 25\text{--}30\%$ in the MP and $\sim 15\%$ in the Taipa Island, indicating lower impacts compared to regional contributions. With regard to PM_{2.5}, estimated proportions of primary vehicular PM_{2.5} emissions are minor, since the atmospheric secondary PM_{2.5} considerably contributed to by vehicle emissions is not considered in this study. It needs to be investigated with a very detailed regional emission inventory including all anthropogenic emission sources and complex air quality models with sophisticated source apportionment functions. This is beyond the scope of this paper. We acknowledge two aspects of uncertainty regarding the AERMOD simulation. First, the strong street canyon effects in the building-dense MP are not sophisticatedly addressed by the AERMOD. Tang and Wang (2007) coupled the OSPM model and detailed building-based geography layer to simulate CO concentrations in the MP under assumed traffic scenarios to address the street canyon effect. Second, the set-up of $500 \text{ m} \times 500 \text{ m}$ cells used in the AERMOD simulation is not adequate for presenting the concentration gradients near major roads and the fine air pollution hotspots. For hotspots, advanced computational fluid dynamics (CFD)-based microscale air quality model coupled with

sophisticated gaseous chemical mechanisms and aerosol dynamics are suggested to quantitatively assess potential impacts and mitigation strategies from perspectives of traffic flows, weather conditions, and architecture layout (Tong et al., 2011).

Usually, ambient NO₂ pollution in the urban area has strong associations with traffic emissions. In Macau, the ambient NO₂ concentration exceedance of the $40 \mu\text{g m}^{-3}$ level was seen in Macau. However, as we note in the methodology section, we do not include the NO₂ results in the paper due to major model limitations of AERMOD (e.g. instantaneous time framework of the basic reaction, inadequate spatial-resolved ambient ozone concentrations, and lacking considerations of other NO_x-related chemical reactions). If the Community Multiscale Air Quality (CMAQ) model, a regional-scale air quality model including regional transport and sophisticated chemical mechanisms, is applied to address these issues, the simulated NO₂ results by using CMAQ would be significantly lower than observed concentrations (see Supplement). Moreover, although a fine grid set-up with a $4 \text{ km} \times 4 \text{ km}$ resolution is used over Macau, only six cells would be created in Macau (note: four cells shared by Macau and Zhuhai together, a city in mainland China and adjacent to Macau). Thereby, advanced air quality simulation technology with finer spatial resolution is required to make use of this link-level emission inventory, since the urban air quality and health impact issues could be very spatially heterogeneous because of the land use policy and the topology of traffic networks. For the congested areas, fleet electrification for diesel fleets such as penetrations of hybrid electric taxis (Wu et al., 2015a) or battery electric buses (Wang et al., 2015)

will help to alleviate ambient NO_2 concentrations in traffic hotspots.

4 Conclusions

High-resolution vehicle emission inventory is a valuable assessment tool to achieve the fine air quality administration, in particular for traffic-populated eastern Asian cities where traffic management is an essential approach to reduce emissions. Due to the difficulties in obtaining link-level traffic flow data and localized emission measurement profiles, such a dedicated environmental tool has not been developed at the link level, which covers a whole city and all vehicle categories. This study selected the entire area of Macau, the most populated city in this world, to demonstrate a high-resolution simulation of vehicular pollution by coupling detailed local data collected and interdisciplinary models (e.g. traffic demand).

Our traffic flow investigation and simulation results showed that total daily traffic activity during a typical weekday of 2010 was estimated at 4.06 million veh km d^{-1} . Passenger trips using MCs, LDPVs, taxis, and buses were responsible for a dominant part of travel demand in Macau, accompanied by a smaller traffic fraction of on-road freight transportation (e.g. trucks) than other cities in mainland China. Spatial heterogeneity of traffic flow characteristics has been discerned between the MP and the remaining parts (i.e. the TCC) of Macau. For example, the MP contributed over 80 % of total traffic accounts in Macau during a weekday of 2010 and MCs were more prevalent in this more populated peninsula compared to the TCC. Tremendous travel demand created during rush hours resulted in significant traffic congestion, indicated by an average speed lower than 15 km h^{-1} for arterial and residential roads in the MP.

Based on a localized vehicle emission model (e.g. the EMBEV-Macau) and high-resolution traffic profiles regarding traffic volume, average speed, and fleet composition, this study established a link-based vehicle emission inventory with high resolution meshed in a temporal and spatial framework (e.g. hourly and link level). We estimated that total daily vehicle emissions in Macau were 16.6 tons of CO, 3.58 tons of THC, 5.00 tons of NO_x , 0.28 tons of $\text{PM}_{2.5}$, and 1001 tons of CO_2 during a typical weekday in 2010. The gasoline fuel CO_2 emissions based on the link-level inventory were in a good agreement with the statistical gasoline consumption record in Macau. MCs are the major contributor to CO and THC emissions due to having higher emission factors than LDPVs. Diesel-powered passenger fleets like buses and taxis contributed 60–65 % of total vehicular emissions of NO_x and $\text{PM}_{2.5}$. With a special focus on the MP region, where traffic density and congestion are more significant, area-specific emission intensity can be higher than the average of the entire Macau area by 135 % for CO, 145 % for THC, 85 % for NO_x , 65 % for $\text{PM}_{2.5}$, and 90 % for CO_2 . The

geographic discrepancy of spatial allocation between THC and $\text{PM}_{2.5}$ emissions can be attributed to the spatially heterogeneous vehicle-use intensity between MCs and diesel fleets (e.g. higher use intensity of MCs in the MP), and this trait could not be identified by using the traditional emission inventory tool. From the perspective of temporal variations, hourly emissions of CO, THC, NO_x , and CO_2 during the evening traffic peak could have been responsible for 7.9–8.7 % of total daily emissions compared to the daily averages when their emission factors were increased by 15–26 % due to the traffic congestion.

We further employed the AERMOD model to quantify average concentrations of CO and $\text{PM}_{2.5}$ contributed by primary vehicle emissions in Macau. Our simulation indicated that receptor-averaged concentrations from primary vehicle emissions were 84.5 ± 86.1 of CO and $1.30 \pm 0.91 \mu\text{g m}^{-3}$ of $\text{PM}_{2.5}$ on weekdays in November 2010. The highest receptor concentrations of CO and $\text{PM}_{2.5}$ were 415 and $4.42 \mu\text{g m}^{-3}$ respectively, all occurring at traffic-populated cells in the MP. Advanced air quality simulation technology with higher spatial resolution and sophisticated chemical transport mechanisms is required to make the use of the link-level emission inventory and better address local air quality issues (e.g. NO_2 pollution). This paper can provide a useful case study and a solid framework for developing high-resolution environmental assessment tools for other vehicle-populated cities in the world. We also highlighted the importance of real traffic data using ITS techniques and the big traffic data approaches to future high-resolution simulation for larger cities in eastern Asia and all over the world.

The Supplement related to this article is available online at doi:10.5194/acp-16-9965-2016-supplement.

Acknowledgements. This work was sponsored by the National High Technology Research and Development Program (863) of China (no. 2013AA065303), the National Natural Science Foundation of China (51322804 and 91544222). We thank Xiao Fu of Tsinghua University for her help in running the CMAQ Model. Shaojun Zhang thanks the Ford Motor Company for supporting the postdoctoral researcher position in University of Michigan. The contents of this paper are solely the responsibility of the authors and do not necessarily represent official views of the sponsors.

Edited by: G. Frost

Reviewed by: two anonymous referees

References

Beijing Transport Research Center: Beijing Transportation Annual Report, available at: www.bjtrc.org.cn (last access: 6 August 2015), 2013.

- Benbrahim-Tallaa, L., Baan, R. A., Grosse, Y., Lauby-Secretan, B., Ghissassi, F. E., Bouvard, V., Guha, N., Loomis, D., and Straif, K.: Carcinogenicity of diesel-engine and gasoline-engine exhausts and some nitroarenes, *Lancet Oncol.*, 13, 663–664, 2012.
- Bishop, G. A., Schuchmann, B. G., Stedman, D. H., and Lawson, D. R.: Multispecies remote sensing measurements of vehicle emissions on Sherman Way in Van Nuys, California, *J. Air Waste Manage. Assoc.*, 62, 1127–1133, 2012.
- Carslaw, D. C., Beevers, S. D., Tate, J. E., Westmoreland, E. J., and Williams, M. L.: Recent evidence concerning higher NO_x emissions from passenger cars and light duty vehicles, *Atmos. Environ.*, 45, 7053–7063, 2011.
- Carslaw, D. C. and Rhys-Tyler, G.: New insights from comprehensive on-road measurements of NO_x, NO₂ and NH₃ from vehicle emission remote sensing in London, UK, *Atmos. Environ.*, 81, 339–347, 2013.
- Chen, Y. and Borcken-Kleefeld, J.: Real-driving emissions from cars and light commercial vehicles, Results from 13 years remote sensing at Zurich/CH, *Atmos. Environ.*, 88, 157–164, 2014.
- Chen, Y. and Borcken-Kleefeld, J.: New emission deterioration rates for gasoline cars, Results from long-term measurements, *Atmos. Environ.*, 101, 58–64, 2015.
- Dallmann, T. R., Kirchstetter, T. W., DeMartini, S. J., and Harley, R. A.: Quantifying on-road emissions from gasoline-powered motor vehicles: Accounting for the presence of medium- and heavy-duty diesel trucks, *Environ. Sci. Technol.*, 47, 13873–13881, 2013.
- Department of Statistics and Census Service (DSEC): Macao, Statistical Information System of Macao, available at: <http://www.dsec.gov.mo/default.aspx> (last access: 15 June 2016), 2014.
- Du, X., Wu, Y., Fu, L., Wang, S., Zhang, S., and Hao, J.: Intake fraction of PM_{2.5} and NO_x from vehicle emissions in Beijing based on personal exposure data, *Atmos. Environ.*, 57, 233–243, 2012.
- EEA (European Environmental Agency): European Union emission inventory report 1990–2012 under the UNECE Convention on Long-range Transboundary Air Pollution (LRTAP), Annex I, European Union (EU-27) LRTAP emission data available at: <http://www.eea.europa.eu/publications/lrtap-2014> (last access: 17 August 2015), 2014.
- Franco, V., Sánchez, F. P., German, J., and Mock, P.: Real-world exhaust emissions from modern diesel cars, The International Council on Clean Transportation Report, available at: <http://www.theicct.org/real-world-exhaust-emissions-modern-diesel-cars> (last access: 6 August 2015), 2014.
- Goh, M.: Congestion management and electronic road pricing in Singapore, *J. Transp. Geogr.*, 10, 29–38, 2002.
- HKCSD (Hong Kong Census and Statistics Department): Hong Kong Statistics, available at: <http://www.censtatd.gov.hk/hkstat/index.jsp> (last access: 17 August 2015), 2014.
- Holmes, N. S. and Morawska, L.: A review of dispersion modelling and its application to the dispersion of particles: An overview of different dispersion models available, *Atmos. Environ.*, 40, 5902–5928, 2006.
- Hu, J., Wu, Y., Wang, Z., Li, Z., Zhou, Y., Wang, H., Bao, X., and Hao, J.: Real-world fuel efficiency and exhaust emissions of light-duty diesel vehicles and their correlation with road conditions, *J. Environ. Sci.*, 24, 865–874, 2012.
- Huo, H., Zhang, Q., He, K., Wang, Q., Yao, Z., and Streets, D.: High-resolution vehicular emission inventory using a link-based method: a case study of light-duty vehicles in Beijing, *Environ. Sci. Technol.*, 43, 2394–2399, 2009.
- Ji, S., Cherry, C. R., Bechle, M. J., Wu, Y., and Marshall, J. D.: Electric vehicles in China: emissions and health impacts, *Environ. Sci. Technol.*, 46, 2018–2024, 2012.
- Lee, T. and Frey, F.: Evaluation of representativeness of site-specific fuel-based vehicle emission factors for route average emissions, *Environ. Sci. Technol.*, 46, 6867–6873, 2012.
- McDonald, B. C., McBride, Z. C., Martin, E. W., and Harley, R. A.: High-resolution mapping of motor vehicle carbon dioxide emissions, *J. Geophys. Res.-Atmos.*, 119, 5283–5298, 2014.
- MEP (Ministry of Environmental Protection, P. R. China): Bulletin of China's Environmental Status in 2013, available at: <http://jcs.mep.gov.cn/hjzl/zkgb/2013zkgb> (last access: 17 August 2015), 2014 (in Chinese).
- Misra, A., Roorda, M. J., and MacLean, H. L.: An integrated modelling approach to estimate urban traffic emissions, *Atmos. Environ.*, 73, 81–91, 2013.
- Murphy, J. G., Day, D. A., Cleary, P. A., Wooldridge, P. J., Millet, D. B., Goldstein, A. H., and Cohen, R. C.: The weekend effect within and downwind of Sacramento – Part 1: Observations of ozone, nitrogen oxides, and VOC reactivity, *Atmos. Chem. Phys.*, 7, 5327–5339, doi:10.5194/acp-7-5327-2007, 2007.
- NBSC (National Bureau of Statistics of China): China Statistical Yearbook, 2014.
- Podrez, M.: An update to the ambient ratio method for 1-h NO₂ air quality standards dispersion modeling, *Atmos. Environ.*, 103, 163–170, 2015.
- Pollack, I. B., Ryerson, T. B., Trainer, M., Parrish, D. D., Andrews, A. E., Atlas, E. L., Blake, D. B., Brown, S. S., Commane, R., Daube, B. C., de Gouw, J. A., Dubé, W. P., Flynn, J., Frost, G. J., Gilman, J. B., Grossberg, N., Holloway, J. S., Kofler, J., Kort, E. A., Kuster, W. C., Lang, P. M., Lefter, B., Lueb, R. A., Neuman, J. A., Nowak, J. B., Novelli, P. C., Peischl, J., Perring, A. E., Roberts, J. M., Santoni, G., Schwarz, J. P., Spackman, J. R., Wagner, N. L., Warneke, C., Washenfelder, R. A., Wofsy, S. C., and Xiang, B.: Airborne and ground-based observations of a weekend effect in ozone, precursors, and oxidation products in the California South Coast Air Basin, *J. Geogr. Res. Atmos.*, 117, D00V05, doi:10.1029/2011JD016772, 2012.
- Saikawa, E., Kurokawa, J., Takigawa, M., Borcken-Kleefeld, J., Mauzerall, D. L., Horowitz, L. W., and Ohara, T.: The impact of China's vehicle emissions on regional air quality in 2000 and 2020: a scenario analysis, *Atmos. Chem. Phys.*, 11, 9465–9484, doi:10.5194/acp-11-9465-2011, 2011.
- Shindell, D., Faluvegi, G., Walsh, M., Anenberg, S. C., van Dingenen, R., Müller, N. Z., Austin, J., Koch, D., and Milly, G.: Climate, health, agricultural and economic impacts of tight vehicle-emission standards, *Nature Climate Change*, 1, 59–66, 2011.
- Tang, U. W. and Wang, Z.: Influences of urban forms on traffic-induced noise and air pollution: Results from a modelling system, *Environ. Model. Softw.*, 22, 1750–1764, 2007.
- Tong, Z., Wang, Y. J., Patel, M., Kinney, P., Chrillrud, S., and Zhang, K. M.: Modeling spatial variations of black carbon particles in an urban highway-building environment, *Environ. Sci. Technol.*, 46, 312–319, 2011.

- Transportation Bureau of Macao (TBM): Consultation report on the road transportation policy planning of Macao 2010–2020, available at: <http://www.dsat.gov.mo/ptt/sc/doc.pdf> (last access: 17 August 2015), 2010
- Transport for London: London Atmospheric Emissions Inventory 2010, Methodology Document, available at: <http://data.london.gov.uk/dataset/london-atmospheric-emissions-inventory-2010> (last access: 12 October 2015), 2014.
- Uherek, E., Halenka, T., Borken-kleefeld, J., Balkanski, Y., Bernsten, T., Borrego, C., Gauss, M., Hoor, P., Juda-Rezler, K., Lelieveld, J., Melas, D., Rypdal, K., and Schmid, S.: Transport impacts on atmosphere and climate: Land transport, *Atmos. Environ.*, 44, 4772–4816, 2010.
- US EPA (US Environmental Protection Agency): AERMOD: Description of model formulation, available at: http://www.epa.gov/scram001/7thconf/aermod/aermod_mfd.pdf (last access: 3 August 2015), 2004.
- US EPA: The 2011 National Emissions Inventory (NEI), available at: <http://www.epa.gov/ttn/chief/net/2011inventory.html> (last access: 23 August 2015), 2014.
- US EPA: Technical support document (TSD) for NO₂-related AERMOD modifications, available at: https://www3.epa.gov/scram001/11thmodconf/AERMOD_NO2_changes_TSD.pdf (last access: 11 June 2016), 2015.
- Velders, G. J. M., Geilenkirchen, G. P., and Lange, R. D.: Higher than expected NO_x emission from trucks may affect attainability of NO₂ limit values in the Netherlands, *Atmos. Environ.*, 45, 3025–3033, 2011.
- Vestreng, V., Ntziachristos, L., Semb, A., Reis, S., Isaksen, I. S. A., and Tarrasón, L.: Evolution of NO_x emissions in Europe with focus on road transport control measures, *Atmos. Chem. Phys.*, 9, 1503–1520, doi:10.5194/acp-9-1503-2009, 2009.
- Vallamsundar, S. and Lin, J.: MOVES and AERMOD used for PM_{2.5} conformity hot spot air quality modeling, *J. Trans. Res. Board*, 2270, 39–48, 2012.
- Walsh, M.P.: PM_{2.5}: global progress in controlling the motor vehicle contribution, *Front. Environ. Sci. Eng.*, 8, 1–17, 2014.
- Wang, H., Fu, L., Lin, X., Zhou, Y., and Chen, J.: A bottom-up methodology to estimate vehicle emissions for the Beijing urban area, *Sci. Total Environ.*, 407, 1947–1953, 2009.
- Wang, R., Wu, Y., Ke, W., Zhang, S., Zhou, B., and Hao, J.: Can propulsion and fuel diversity for the bus fleet achieve the win-win strategy of energy conservation and environmental protection?, *Appl. Energ.*, 147, 92–103, 2015.
- Wang, X., Westerdahl, D., Wu, Y., Pan, X., and Zhang, K. M.: On-road emission factor distributions of individual diesel vehicles in and around Beijing, China, *Atmos. Environ.*, 45, 503–513, 2011.
- Wang, X., Westerdahl, D., Hu, J., Wu, Y., Yin, H., Pan, X., and Zhang, K. M.: On-road diesel vehicle emission factors for nitrogen oxides and black carbon in two Chinese cities, *Atmos. Environ.*, 46, 45–55, 2012.
- Wang, Z., Wu, Y., Zhou, Y., Li, Z., Wang, Y., Zhang, S., and Hao, J.: Real-world emissions of gasoline passenger cars in Macao and their correlation with driving conditions, *Int. J. Environ. Sci. Technol.*, 11, 1135–1146, 2014.
- Wu, Y., Wang, R., Zhou, Y., Lin, B., Fu, L., He, K., and Hao, J.: On-Road vehicle emission control in Beijing: past, present, and future, *Environ. Sci. Technol.*, 45, 147–153, 2011.
- Wu, X., Zhang, S., Wu, Y., Un, P., Ke, W., Fu, L., and Hao, J.: On-road measurement of gaseous emissions and fuel consumption for two hybrid electric vehicles in Macao, *Atmos. Pollut. Res.*, 6, 858–866, 2015a.
- Wu, X., Zhang, S., Wu, Y., Li, Z., Fu, L., and Hao, J.: Real-World Emissions and Fuel Consumption of Diesel Buses and Trucks in Macao: From On-road Measurement to Policy Implications, *Atmos. Environ.*, 120, 393–403, 2015b.
- Wu, X., Wu, Y., Zhang, S., Liu, H., Fu, L., and Hao, J.: Assessment of vehicle emission programs in China during 1998–2013: achievement, challenges and implications, *Environ. Pollut.*, 214, 556–567, 2016.
- Wu, Y., Zhang, S. J., Li, M. L., Ge, Y. S., Shu, J. W., Zhou, Y., Xu, Y. Y., Hu, J. N., Liu, H., Fu, L. X., He, K. B., and Hao, J. M.: The challenge to NO_x emission control for heavy-duty diesel vehicles in China, *Atmos. Chem. Phys.*, 12, 9365–9379, doi:10.5194/acp-12-9365-2012, 2012.
- Zannetti, P.: *Air Pollution Modeling*, Springer US, 1990.
- Zhang, S., Wu, Y., Liu, H., Wu, X., Zhou, Y., Yao, Z., Fu, L., He, K., and Hao, J.: Historical evaluation of vehicle emission control in Guangzhou Based on a multi-year emission inventory, *Atmos. Environ.*, 76, 32–42, 2013.
- Zhang, S., Wu, Y., Wu, X., Li, M., Ge, Y., Liang, B., Xu, Y., Zhou, Y., Liu, H., Fu, L., and Hao, J.: Historic and future trends of vehicle emissions in Beijing, 1998–2020: A policy assessment for the most stringent vehicle emission control program in China, *Atmos. Environ.*, 89, 216–219, 2014a.
- Zhang, S., Wu, Y., Liu, H., Huang, R., Un, P., Zhou, Y., Fu, L., and Hao, J.: Real-world fuel consumption and CO₂ (carbon dioxide) emissions by driving conditions for light-duty passenger vehicles in China, *Energy*, 69, 247–257, 2014b.
- Zhang, S., Wu, Y., Liu, H., Huang, R., Yang, L., Li, Z., Fu, L., and Hao, J.: Real-world fuel consumption and CO₂ emissions of urban public buses in Beijing, *Appl. Energ.*, 113, 1645–1655, 2014c.
- Zhang, S., Wu, Y., Hu, J., Huang, R., Zhou, Y., Bao, X., Fu, L., and Hao, J.: Can Euro V heavy-duty diesel engines, diesel hybrid and alternative fuel technologies mitigate NO_x emissions? New evidence from on-road tests of buses in China, *Appl. Energ.*, 132, 118–126, 2014d.
- Zheng, X., Wu, Y., Jiang, J., Zhang, S., Liu, H., Song, S., Li, Z., Fan, X., Fu, L., and Hao, J.: Characteristics of on-road diesel vehicles: Black carbon emissions in Chinese cities based on portable emissions measurement. *Environ. Sci. Technol.*, 49, 13492–13500, 2015.
- Zheng, X., Wu, Y., Zhang, S., Baldauf, R. W., Zhang, K. M., Hu, J., Li, Z., Fu, L., and Hao, J.: Joint measurements of black carbon and particle mass for heavy-duty diesel vehicles using a portable emission measurement system, *Atmos. Environ.*, 141, 435–442, 2016.
- Zhou, Y., Wu, Y., Yang, L., Fu, L., He, K., Wang, S., Hao, J., Chen, J., and Li, C.: The impact of transportation control measures on emission reductions during the 2008 Olympic Games in Beijing, China, *Atmos. Environ.*, 44, 285–293, 2010.
- Zhou, Y., Wu, Y., Zhang, S., Fu, L., and Hao, J.: Evaluating the emission status of light-duty gasoline vehicles and motorcycles in Macao with real-world remote sensing measurement, *J. Environ. Sci.*, 26, 2240–2248, 2014.